Soft Matter

ARTICLE TYPE

Cite this: DOI: 00.0000/xxxxxxxxxx

Electronic Supplemental Information for "Relative effects of polymer composition and sample preparation on glass dynamics"

Robert M. Elder[a*], Amanda L. Forster[b], Ajay Krishnamurthy[b], Joseph M. Dennis[c], Hiroshi Akiba[d], Osamu Yamamuro[d], Kanae Ito[e], Katherine M. Evans[f], Christopher Soles[f], Timothy W. Sirk[c*]

Received Date
Accepted Date

DOI: 00.0000/xxxxxxxxxx

1 Additional Simulation Details

Composition. The simulated polymers were built from ENB and NBOH repeat units. The least polar chemistry is pure ENB with 20 ENB monomers per chain. From there, we increased the polarity by replacing 5, 10, 15, or all 20 of the ENB monomers with NBOH. These ENB-*co*-NBOH copolymers are termed $\phi_{ENB} = 100$, 75, 50, 25, 0% ENB, respectively. The monomers were randomly distributed along the chains. For each copolymer, five chains with distinct random ordering were generated. We packed 64 of each distinct chain into the simulation cell to create a large system with 320 chains. These systems contained exactly 136,000 atoms, a relatively large volume compared with the void volumes of interest. As in prior work,[1–3] we quantified the polarity via the octanol-water partition coefficient $\log P$ normalized by molecular surface area SA. Low $\log P/SA$ indicates high hydrophilicity or polarity.

Forcefield and equation of motion. The general Amber force field (GAFF, version 2.1) was used for all systems.[4,5] Short-range non-bonded interactions were cut off at 9 Å, and long-range contributions of van der Waals interactions to the energy and pressure were estimated using tail corrections.[6] Atomic partial charges were calculated using the AM1-BCC method.[7,8] Electrostatic interactions were calculated using the particle-particle particle-mesh (PPPM) method.[9] The velocity-Verlet integrator was used with a timestep of 1.0 fs. Temperature and pressure were controlled with a Nosé-Hoover thermostat and barostat with damping constants of 0.1 and 1.0 ps, respectively.[10] Isotropic pressure control was used to maintain 1 atm pressure. The simulation box was periodic in three dimensions. We employed the LAMMPS simulation package[11] (http://lammps.sandia.gov) for all simulations. VMD was used for visualization.[12]

Sample preparation. After construction, the systems were equilibrated with isothermal-isobaric (*NPT*) MD simulation at 700 K for 1 ns. The structures were then slowly relaxed into the glassy state using incremental cooling. The temperature was reduced in steps of 20 K, with a short *NPT* MD simulation performed at each new temperature, until the system was in the glassy state at 300 K. The duration of the short *NPT* MD simulation was chosen to set the cooling rate: 200 ps for 10^{11} K/s, 20 ps for 10^{12} K/s, and 2 ps for 10^{13} K/s. Five replica structures were created for each chemistry, using different initial positions and velocities such that the replicas have different structures. Error bars are the standard deviation of these five replicas. Molecular structures were generated at the experimental density via hydrostatic compression after the initial quench to 300 K, as follows: starting from structures quenched at 10^{11} K/s, the box volume was affinely scaled to the experimental density over 1 ns. We term this protocol 'quench-then-compress' (QtC), which is referred to as $\dot{q} = 10^0$ K/s in the manuscript. To verify that the void volume distribution is not overly sensitive to this protocol, we also performed the opposite 'compress-then-quench' (CtQ). In CtQ, the system is scaled to the correct density at high T and then quenched to 300 K at 10^{11} K/s. The void distributions in the final structure were similar. Full distributions are shown in Figure S1.

[a]*current address: Center for Devices and Radiological Health, U.S. Food and Drug Administration, Silver Spring, Maryland 20903, United States; E-mail: robert.elder@fda.hhs.gov*
[b]*Materials Measurement Science Division, National Institute of Standards and Technology, Gaithersburg, Maryland 20899, United States*
[c]*Polymers Branch, U.S. DEVCOM Army Research Laboratory, Aberdeen Proving Ground, Maryland 21005, United States; E-mail: timothy.w.sirk.civ@army.mil*
[d]*Institute for Solid State Physics, University of Tokyo, Kashiwa, Chiba, 277-8581, Japan*
[e]*Industrial Application Division, Spring-8, Japan Synchrotron Radiation Research Institute (JASRI), 1-1-1 Kouto, Sayo, Hyogo 679-5198, Japan*
[f]*Materials Science and Engineering Division, National Institute of Standards and Technology, Gaithersburg, Maryland 20899, United States*

Additional results. Distributions of void volume from the simulations are given for all quench rates and compositions in Figure S2. Similarly, all MSD curves from simulations are provided in Figure S3, where $\langle \Delta r^2(t) \rangle$ is computed by averaging over the self-diffusion for each atom i as

$$\langle \Delta r^2(t) \rangle = \left\langle \left[r_i(t_0+t) - r_i(t_0) \right]^2 \right\rangle. \quad (1)$$

The MSD curves shown in Fig. S3 and results given in the main text are averaged over all replica structures and reference times t_0.

Figure S4 shows a comparison of void volume distributions for systems with varying composition and quench rate but with similar average void volumes. The distributions are generally similar for small voids. Figure S5 shows a comparison between the Debye-Waller factor $\langle u^2 \rangle$ obtained from simulations and experiments for $\phi_{ENB} = 0.0$, 0.5, and 1.0. Figure S6 gives an example calculation of α at 500 K ($T \gg T_g$).

2 Additional Experimental Details

Quasi-elastic neutron scattering (QENS) measurements were performed on the angle focusing neutron spectrometer, AGNES, on the cold neutron guide (C3-1-1) at the Japan Atomic Energy Agency's Japanese Research Reactor 3 (JRR-3).[13] This cold neutron time-of-flight spectrometer, a part of the University of Tokyo's Institute for Solid State Physics, was operated in the "high resolution mode," selecting a neutron wavelength of 5.5 Å, which corresponds to an elastic peak energy resolution of 0.04 meV at full width half max. Given this energy resolution, relaxation processes longer than approximately 10 ps appear static. At these settings the AGNES spectrometer can nominally access a Q range of approximately (0.15 to 2.1) Å^{-1}. Full inelastic neutron scattering spectra were collected at 8 hours per spectrum for the following samples and temperatures (K):

ϕ_{ENB} = 1.0: 4, 100, 150, 200, 250, 300, 350
ϕ_{ENB} = 0.5: 100, 200, 300
ϕ_{ENB} = 0.0: 4, 100, 150, 200, 250, 300, 350

In this publication we limit our analysis of the QENS spectra to the elastic scattering intensities to quantify a mean-square atomic displacement, $\langle u^2 \rangle$, that can be compared to the molecular dynamics simulations presented in the main text of this manuscript. At these low temperatures, the elastic scattering intensities (IE) were relatively weak and did not warrant breaking the QENS spectra into multiple bins of Q. Rather than the conventional plotting of $\log(I_{el})$ vs Q^2 to extract $\langle u^2 \rangle$ at each T from the slope, we integrated the values of I_E over all of the available Qs into $I_{E-total}$. We then plot the relative mean square displacements in terms of $\langle u^2(T) \rangle - \langle u^2(5K) \rangle$ from $[\log(I_{E-total}(T)) - \log(I_{E-total}(5K))]/Q^2_{ave}$ where $Q^2_{ave} \approx 1.0$ Å^{-1}.

Figure S7 below shows an example of the elastic peaks in the QENS data as a function of temperature for the ϕ_{ENB}=1.0 resin. Data for the ϕ_{ENB}= 0.5 and 0.0 resins are qualitatively similar and not shown here. The vertical lines between -0.14 and +0.08 meV give the energy limits over which the IE was integrated. Figure S8 then correspondingly shows how $I_{E-total}$ varies across the different temperatures and compositions studied. The intensity variation among the three samples is due to the difference in sample quantity. These values were then used to calculate the relative mean square displacement, $\langle u^2(T) \rangle - \langle u^2(5K) \rangle$, as a function of T, as shown in Figure S9. The $\langle u^2(T) \rangle - \langle u^2(5K) \rangle$ at 300 K are taken from this plot and overlaid onto Figure 3d in the main portion of the manuscript. The $\langle u^2 \rangle$ values of the sample with $\phi_{ENB} = 1.0$ are smaller than expected at higher temperatures. This may be because the Q region for the integration is limited to 0.5-2.1 Å^{-1}. That is, the spatial range for the motion of the sample with $\phi_{ENB} = 1.0$ may spread, especially to the low-Q region. Given the energy resolution of the spectrometer, it is important to realize that $\langle u^2(T) \rangle - \langle u^2(5K) \rangle$ integrates motions that are faster than 10 ps, but with an emphasis on the lower frequency motions in the integral. In the fullest representation for the harmonic vibrations in a crystal, $\langle u^2 \rangle$ in a neutron scattering experiment is a frequency weighted integral over the vibrational density of states within the sample:

$$\langle u^2 \rangle = \frac{3\hbar}{2M} \int_0^{\omega_m} \frac{1}{\omega} \coth\left(\frac{1}{2}\omega\beta\right) Z(\omega) d\omega \quad (2)$$

In this equation, $Z(\omega)$ is the phonon density of states in the sample as a function of frequency of motion ω, M is the molar mass, and β is $1/k_bT$.[14] When this integration is performed, we find that the frequency dependence of $\langle u^2 \rangle$ reduces to:

$$\langle u^2 \rangle \sim \frac{Z(\omega)}{\omega^2} \quad (3)$$

This illustrates that the lowest frequency motions in the system dominate $\langle u^2 \rangle$, which makes intuitive sense. High frequency (energy) motions tend to be more localized, with small displacements, in comparison to low frequency (energy) motions that tend to be more extensive and delocalized. Therefore it is reasonable to expect that the motions reflected in $\langle u^2(T) \rangle - \langle u^2(5K) \rangle$ are dominated by the slowest 10 ps motions that can be resolved by the AGNES spectrometer.

Notes and references

1 R. M. Elder, T. R. Long, E. D. Bain, J. L. Lenhart and T. W. Sirk, *Soft Matter*, 2018, **14**, 8895–8911.
2 A. J. D. Magenau, J. A. Richards, M. A. Pasquinelli, D. A. Savin and R. T. Mathers, *Macromolecules*, 2015, **48**, 7230–7236.
3 E. Yildirim, D. Dakshinamoorthy, M. J. Peretic, M. A. Pasquinelli and R. T. Mathers, *Macromolecules*, 2016, **49**, 7868–7876.
4 J. Wang, R. M. Wolf, J. W. Caldwell, P. A. Kollman and D. A. Case, *J. Comput. Chem.*, 2004, **25**, 1157–1174.
5 J. Wang, W. Wang, P. A. Kollman and D. A. Case, *J. Mol. Graphics Modell.*, 2006, **25**, 247–260.
6 H. Sun, *J. Phys. Chem. B*, 1998, **102**, 7338–7364.
7 A. Jakalian, B. L. Bush, D. B. Jack and C. I. Bayly, *J. Comput. Chem.*, 2000, **21**, 132–146.
8 A. Jakalian, D. B. Jack and C. I. Bayly, *J. Comput. Chem.*, 2002, **23**, 1623–1641.

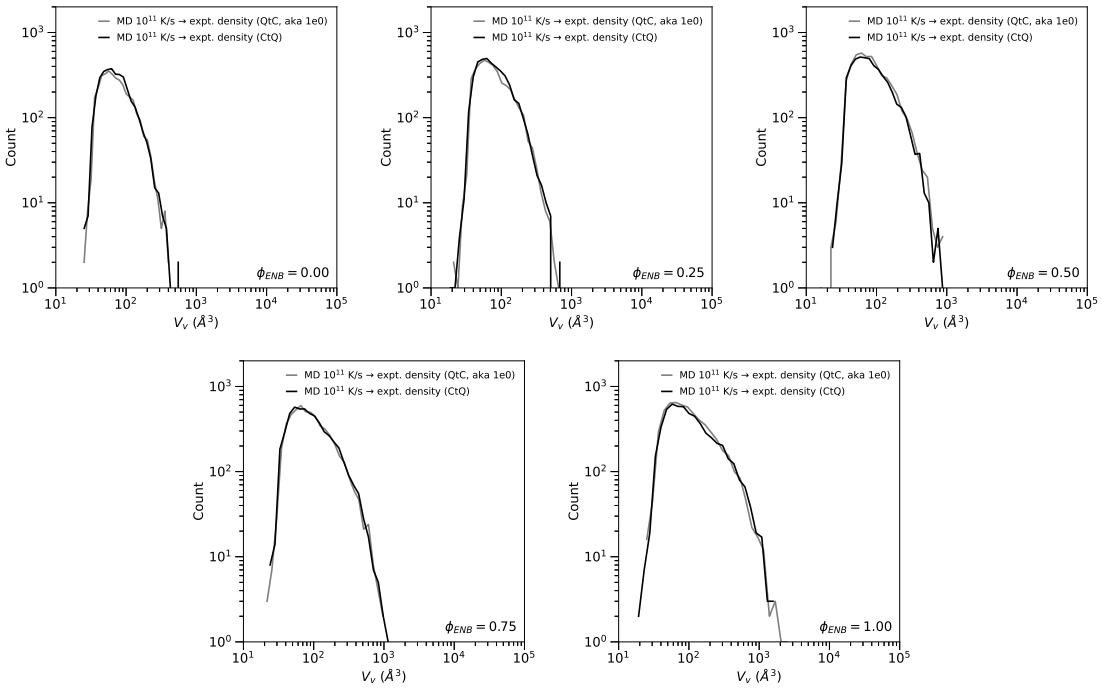

Fig. S1 Void volume $\langle v_v \rangle$ distributions from simulations for all compositions ϕ_{ENB} and using the QtC (i.e., $\dot{q} = 10^0$ K/s in the manuscript) and CtQ protocols with a quench rate of 10^{11} K/s and the target density chosen to match the experimental value.

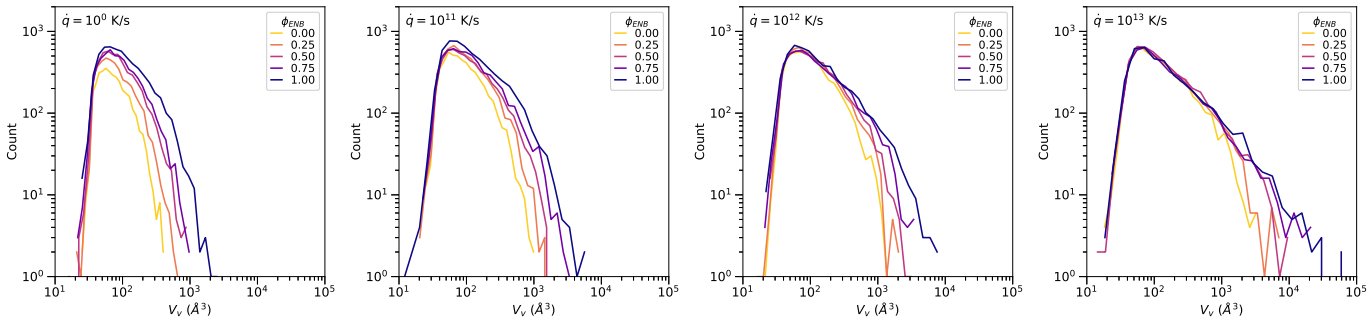

Fig. S2 Void volume $\langle v_v \rangle$ distributions from simulations for all compositions ϕ_{ENB} and quench rates $\dot{q}$.

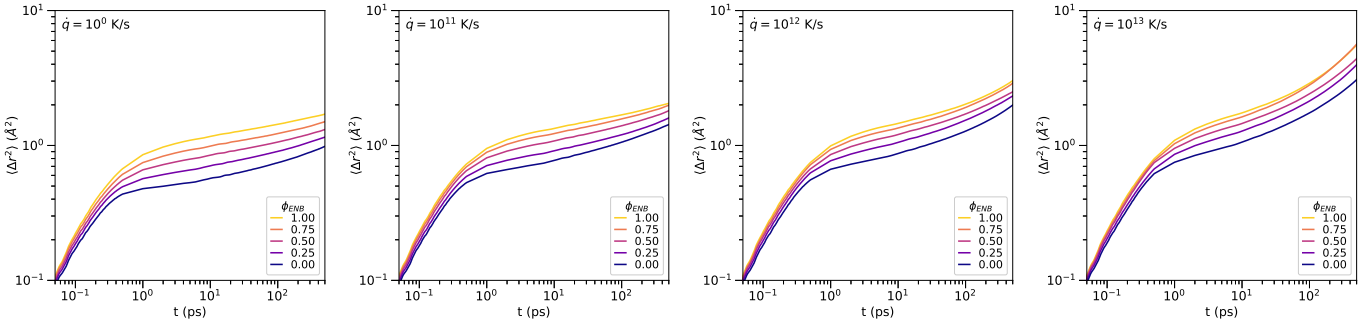

Fig. S3 Mean-squared displacements $\langle \Delta r^2 \rangle$ from simulations for all compositions ϕ_{ENB} and quench rates $\dot{q}$.

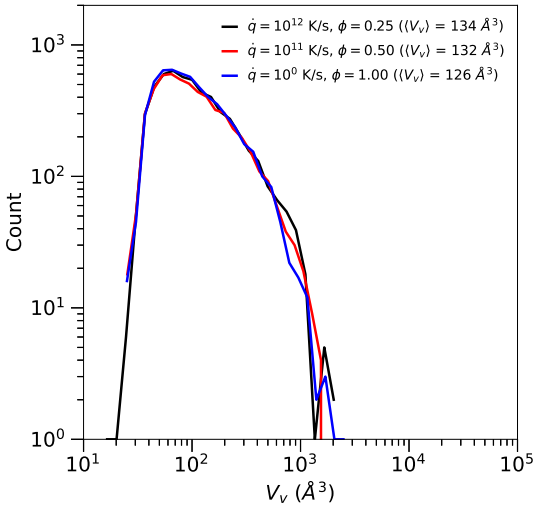

Fig. S4 Comparison of void volume $\langle v_v \rangle$ distributions from simulations with compositions ϕ_{ENB} and quench rates $\dot{q}$ with similar average void volume $\langle V_v \rangle$.

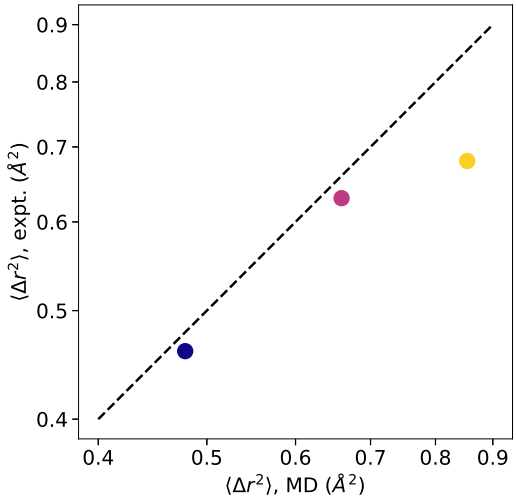

Fig. S5 Comparison of the Debye-Waller factor $\langle u^2 \rangle$ obtained from simulations and experiments for $\phi_{ENB} = 0.0$, 0.5, and 1.0. The dashed line indicates equality between the x and y axes.

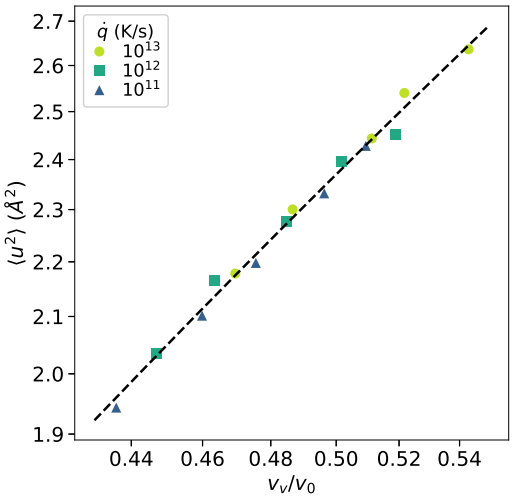

Fig. S6 The Debye-Waller factor vs void fraction at 500 K ($T >> T_g$), given as a log-log plot. The dashed line is a fit to a power law $\langle u^2 \rangle \sim (v_v/v_0)^{2/\alpha}$ with the exponent $\alpha \approx 3/2$.

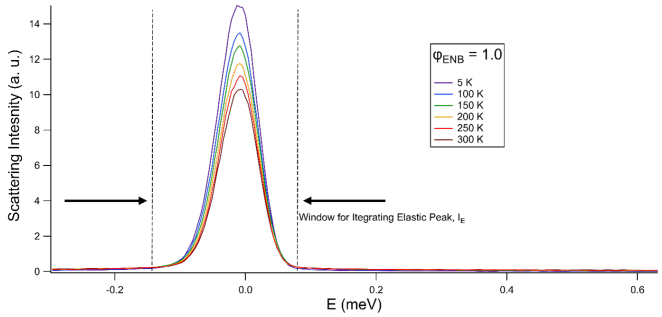

Fig. S7 Full QENS spectra as a function of T for the $\phi_{ENB} = 0.0$ sample. Vertical lines indicate the limits over which the strong central elastic peak intensities were integrated.

9 R. W. Hockney and J. W. Eastwood, *Computer simulation using particles*, Institute of Physics Publishing, Philadelphia, 1988, p. 564.

10 W. Shinoda, M. Shiga and M. Mikami, *Phys. Rev. B*, 2004, **69**, 134103.

11 S. Plimpton, *J. Comput. Phys.*, 1995, **117**, 1–19.

12 W. Humphrey, A. Dalke and K. Schulten, *J. Mol. Graphics*, 1996, **14**, 33–38.

13 T. Kajitani, K. Shibata, S. Ikeda, M. Kohgi, H. Yoshizawa, K. Nemoto and K. Suzuki, *Physica B: Condensed Matter*, 1995, **213**, 872–874.

14 G. Squires, *Introduction to the Theory of Thermal Neutron Scattering by GL Squires*, 1996.

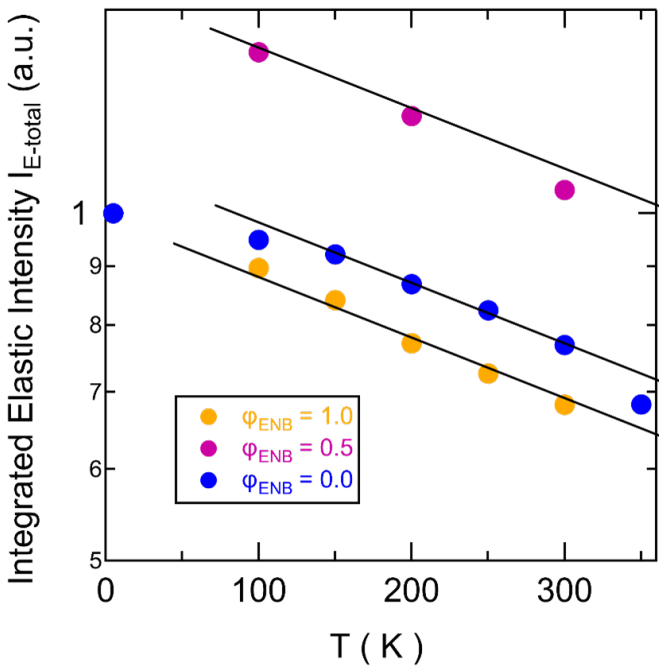

Fig. S8 Integrated total elastic peak intensities $I_{E-total}$ for the different ENB compositions ϕ_{ENB} and temperatures T studied here. Straight lines are simple guides to the eye.

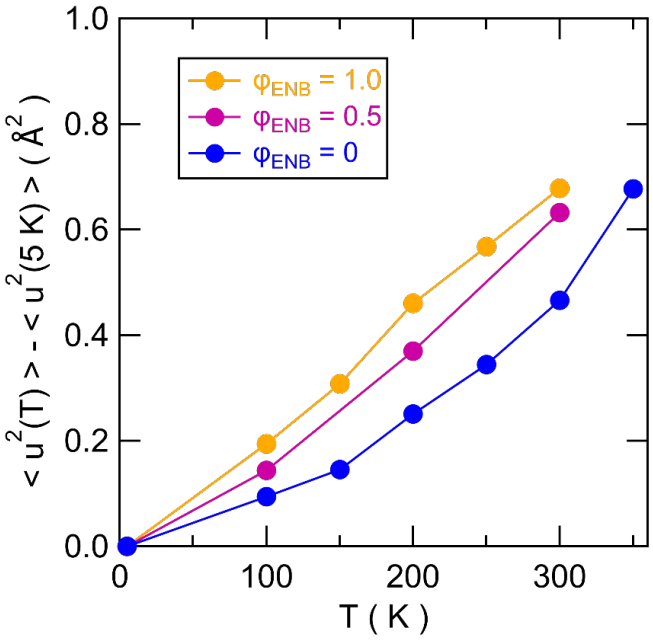

Fig. S9 Relative mean-square displacements $\langle u^2(T)\rangle - \langle u^2(5K)\rangle$ for the different ENB compositions ϕ_{ENB} and temperatures T studied here.